Windproofing LIGO: Improving low-frequency active seismic isolation using rotation sensors.

Krishna Venkateswara[1*], Jim Warner[2], Michael P. Ross[1], Conor Mow Lowry[3], Brian Lantz[4], Jeffrey Kissel[2] , Hugh Radkins[2], Thomas Shaffer[2], Richard Mittleman[5], Sam Cooper[3],and Arnaud Pele[6]

E-mail: kvenk@uw.edu*
University of Washington[1], LIGO Hanford Observatory[2], University of Birmingham[3], Stanford University[4], MIT[5], LIGO Livingston Laboratory[6]

Note

DCC number P1800038

Abstract. Modern gravitational-wave observatories require robust low-frequency active seismic isolation in order to keep the interferometer operating stably at their ideal operating point at all times. To ensure good seismic isolation from microseismic motion, seismometers are used to measure ground or platform acceleration at frequencies below 0.1 Hz, which makes them susceptible to acceleration from ground tilt, particularly arising from wind-pressure acting on building walls. Consequently, both LIGO observatories suffered significant downtime under wind-speeds above 7 m/s in the first observation run. We describe the use of ground rotation sensors at LIGO Hanford Observatory to correct nearby ground seismometers, thus producing a tilt-free ground displacement signal. Using these signals for feedforward isolation of the optical platforms enabled a robust low-frequency seismic isolation, which allowed gravitational wave observation time under wind speeds as high as $15 - 20$ m/s during the second observation run.

PACS numbers: 07.10.Fq

Submitted to: *Class. Quantum Grav.*

1. Introduction

During the first observation run of the Advanced Laser Interferometer Gravitational-wave Observatory (LIGO), multiple gravitational-wave candidates were detected over a 16-week-long duration [1]. The duty-cycle of the LIGO Hanford Observatory (LHO) and the LIGO Livingston Observatory (LLO) was 67.6% and 57.4% respectively with significant downtime due to high wind and microseismic motion [2]. Even when the interferometers were operational, significant excess noise was observed in the detectors during wind-speeds exceeding 7 m/s.

To keep the interferometer locked and operating at the optimum point, the net differential motion of the suspended test-masses in the two arm-cavities needs to be less than 10^{-14} m rms. The differential ground motion over 4-km has a strong frequency dependence and variability with time. Fig. 1 shows an example of ground motion at LHO near the input and end test masses and the differential motion between the two, measured when the wind speeds were below 3 m/s. As will be seen later, wind-induced ground tilt can dominate the ground motion below 0.1 Hz. Between 0.05 to 0.5 Hz, the ground motion is largely dictated by Rayleigh surface waves arising from the pressure of interacting ocean waves on the sea floor [3]. The $10 - 15$-s-period ocean waves produce the so-called primary, secondary and tertiary microseism peaks through interference effects. The amplitude of the secondary is usually the largest and can vary from $\sim 0.1 - 3$ μm depending on ocean activity and location on the continents. It is also worth noting that the differential ground motion over the 4-km arm at LIGO is reduced significantly between 0.05 to 0.2 Hz, since the wavelength of the seismic waves at these frequencies is ~ 40 km. At the diurnal and semi-diurnal frequency, the tides can produce between $100 - 250$ μm of differential displacement over the arms. To keep the interferometer locked stably, multiple feedback loops are engaged to minimize the length and angular fluctuations of the test mass cavities.

The data and analysis in this paper is limited to LHO, which was the only site that received tilt-sensors between the first and second observing runs. The ground motion at the two LIGO sites has certain differences (due to the location and ground properties) which make it difficult to immediately apply the following filters and

sensors to LLO. Nevertheless, similar schemes could be applied to both LIGO sites and other gravitational-wave detectors.

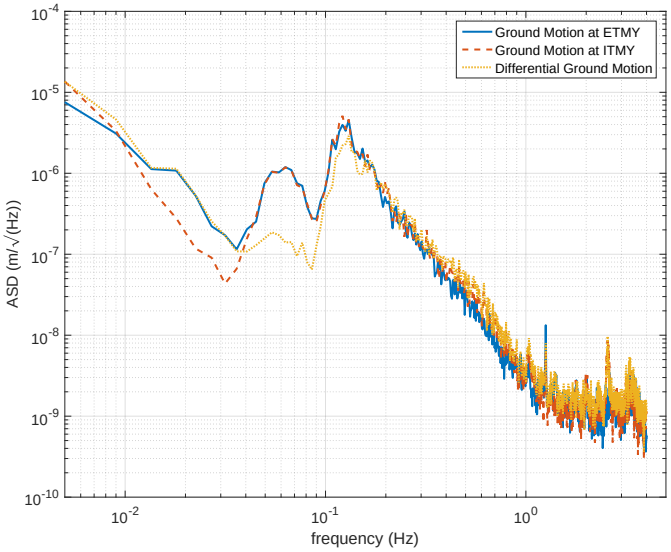

Figure 1. Amplitude spectral density (ASD) of the ground motion along the Y-arm at LHO, measured near the input (ITMY) and end (ETMY) test masses and the differential motion between the two. The primary and secondary microseismic peaks are clearly visible between 0.05 to 0.5 Hz.

1.1. Platform Control Configuration

The active isolation system in LIGO is described in detail in [4]. In general, the suspended platform can be controlled by feedback using on-board mounted sensors or feedforward using sensors on the ground. When viewed locally, these two approaches are nearly equivalent if the sensors are the same, but using on-board sensors for feedback is slightly superior since there may be differences between motion sensed at the ground sensor and the motion affecting the platform. In the first Observation run of LIGO, we adopted the strategy of using just the on-board sensor for feedback cancellation of the platform motion down to 50 mHz, referred to in this paper as the O1 Configuration. After O1, two ground-rotation-sensors [5] installed at the two end-stations at LHO were used for tilt-subtraction from the ground seismometers [6]. Interestingly, it was found that the tilt sensed by the corner-station seismometer was significantly less than the end-station seismometers under similar wind-speeds. This is likely due to the fact that it is situated much further from the building walls than is possible at the end-stations. Thus the tilt-subtracted seismometers at the end-stations and a tilt-free seismometer at the corner stations constituted a set of low-tilt seismometers. For the second observing run, a strategy of using a combination of the low-tilt ground seismometers for feedforward at low frequencies and using the on-board sensors for feedback at high frequencies was adopted, referred to as the O2

Configuration.

The drawback of the O1 configuration is that it was found to increase the platform motion dramatically as ground tilt increased due to winds acting on the building walls. It also fails to take advantage of the fact that ground motion in the 50-150 mHz range (due to the microseisms) are correlated over the 4-km arms of the interferometer and highly correlated over few the tens of meters separation for the corner station chambers. The main reason in both cases is due to the poor sensitivity of the on-platform tilt sensor, which consists of differential vertical seismometers.

2. Simple Analytical Model

The active isolation of the main test-mass employs two main subsystems- HEPI and ISI. (More explanation needed) The analytical model considered below describes the isolation achieved by the first stage of the ISI, which accounts for most of the low-frequency performance of the system. This calculation follows the procedure outlined in [7]. While this model lacks the full complexity and ability to incorporate cross-couplings of a numerical model, it is nevertheless instructive in understanding the main features of the system and guiding the development of feedforward filters.

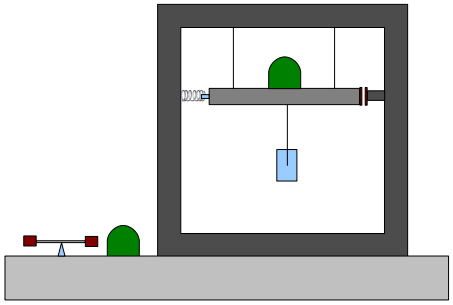

Figure 2. Schematic representation of the Internal Seismic Isolation stage showing the optic (light blue) hanging from the seismic isolation platform (gray) which is contained within the vacuum chamber (dark gray). The three types of sensors, seismometers (green), tilt-sensor (copper ended bar), and capacitive positions sensor (black plates) are shown along with the magnetic actuator (coil).

Fig. 2 shows a simplified schematic of the ISI which includes the on-board seismometer (T240), capacitative position sensor (CPS), the ground seismometer (STS2), and the ground tilt-sensor (BRS). Fig. 3 and Fig. 4 describes the design of the control loop for the tilt and translation-degrees of freedom.

In the limit of large loop gains and at low frequencies where the plant dynamics are unimportant, the equations governing the platform translation and tilt with respect to the ground translation, tilt inputs, and sensor noises can be shown to be the following.

The platform translation due to ground translation can be expressed as

$$x_p = F_{LP,x} \cdot (1 - F_{SC,x}) \cdot g_x. \tag{1}$$

Where g_x is the ground translation, x_p is the platform translation, $F_{LP,x}$ and $F_{SC,x}$ are respectively a low pass filter and the sensor correction filter.

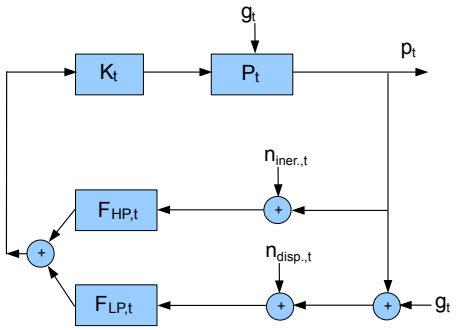

Figure 3. Model of the tilt control loop for Stage 1 of the ISI. Where g_t is the ground tilt, p_t is the platform tilt, $n_{iner.,t}$ and $n_{disp.,t}$ are the tilt noise for the on-board T240 pair and CPS respectively, $F_{HP,t}$ and $F_{LP,t}$ are respectively high pass and low pass filters, K_t is the feedback filter, and P_t is the platform tilt transfer function.

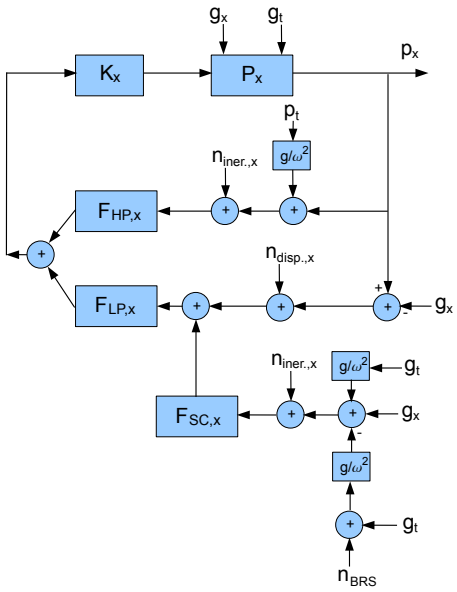

Figure 4. Model of the translation control loop for Stage 1 of the ISI. Where g_t and g_x are the ground tilt and ground translation respectively, p_x and p_t are the platform translation and tilt, $n_{iner.,x}$, $n_{disp.,x}$ and n_{BRS} are the noise for the on-board T240, CPS, and BRS respectively, $F_{HP,x}$, $F_{LP,x}$, and $F_{SC,x}$ are respectively a high pass filter, a low pass filter, and the sensor correction filter, K_x is the feedback filter, and P_x is the platform translation transfer function.

Ground tilt can produce platform translation through the following two terms:

$$x_p = -F_{LP,x} \cdot F_{SC,x} \cdot \frac{g}{\omega^2} \cdot g_{tilt} - F_{HP,x} \cdot \frac{g}{\omega^2} \cdot F_{LP,t} \cdot g_{tilt}. \tag{2}$$

Where g_{tilt} is the ground tilt, x_p is the platform translation, $F_{HP,x}$, $F_{LP,x}$, and $F_{SC,x}$ are respectively a high pass filter, a low pass filter, and the sensor correction filter, g is the gravitational acceleration, and ω is the frequency of motion. The first term is due to the tilt-sensitivity of the ground seismometer and the second is due to the platform tilt being sensed as translation by the platform seismometer.

When a tilt sensor is used to subtract tilt from the ground sensor, the ground tilt in the first term is replaced with the level of noise in the tilt-subtracted channel. Ideally this would be dictated by the sensor noise in the BRS and the seismometer. In reality, the tilt-subtracted residual signal is known to be limited by the differences in tilt sensed by the two sensors. Hence a signal-dependent 'noise' is added to account for the extra noise in the tilt-subtracted channel. Therefore with the use of the BRS, eq. 2 is modified as follows:

$$x_p = -F_{LP,x} \cdot F_{SC,x} \cdot \frac{g}{\omega^2} \cdot n_{TS} - F_{HP,x} \cdot \frac{g}{\omega^2} \cdot F_{LP,t} \cdot g_{tilt}. \tag{3}$$

where the noise in the tilt-subtracted channel n_{TS} is modelled as

$$n_{TS} = -n_{BRS} + \alpha \cdot g_{tilt} \tag{4}$$

Where α is the residual tilt factor which in the current sensor scheme is $\sim \frac{1}{10}$. The sum of sensor noises affecting the platform translation can be written as

$$\begin{aligned} x_p = & -F_{HP,x} \cdot n_{iner.,x} - F_{LP,x} \cdot n_{disp.,x} \\ & - F_{LP,x} \cdot F_{SC,x} \cdot n_{iner.,x} + F_{HP,x} \cdot \frac{g}{\omega^2} \cdot F_{HP,t} \cdot n_{iner.,t} \\ & + F_{HP,x} \cdot \frac{g}{\omega^2} \cdot F_{LP,t} \cdot n_{disp.,t} \end{aligned} \tag{5}$$

Where x_p is the platform translation, $n_{iner.,x}$ and $n_{disp.,x}$ are the translation noise for the on-board T240 and CPS respectively, $n_{iner.,t}$ and $n_{disp.,t}$ are the tilt noise for the on-board T240 pair and CPS respectively. Similarly, the platform tilt arising due to ground tilt is

$$t_p = F_{LP,t} \cdot g_t. \tag{6}$$

And the platform tilt due to the sum of sensor noises is

$$t_p = -F_{HP,t} \cdot n_{iner.,t} - F_{LP,t} \cdot n_{disp.,t}. \tag{7}$$

To study the effects of these filters on the system, we construct an idealized model of the translation and tilt inputs to the system. Fig. 5 shows the Amplitude Spectral Density (ASD) of the modeled ground translation and ground tilt sensed as translation under low and high wind conditions (wind-speeds of $10 - 12$ m/s) along with various sensor noise models. The assumption here is that the ground translation remains the same under high wind, but it is only the increased tilt which increases the sensed translation. Similarly Fig. 6 shows the ground tilt under low wind and high wind conditions.

Using these models and Eqs. 1-7, we can compute the platform responses in translation and tilt for the two control strategies. Fig. 7 shows the platform tilt under low wind conditions with the O1 configuration. The control performance is limited by the Stage 1 CPS sensor noise below $\sim$ 500 mHz.

Fig. 8 shows the translation of the platform under low wind conditions. At frequencies above $\sim$ 0.8 Hz, the platform achieves a nearly sensor-noise-limited isolation performance. At lower frequencies, the translation of the platform is dominated by residual ground motion and is limited by the low-pass in the blend

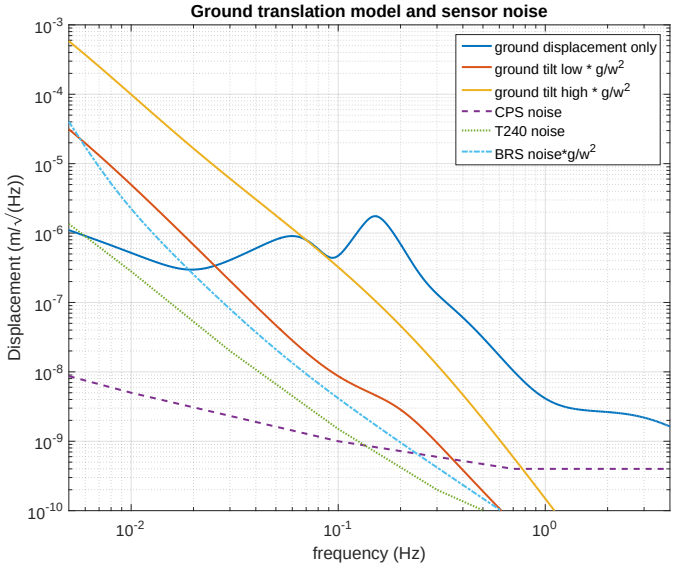

Figure 5. ASD of the modeled ground translation, along with low and high tilt models converted to translation units. Also shown are translational sensor noise models for the CPS, T240, and BRS.

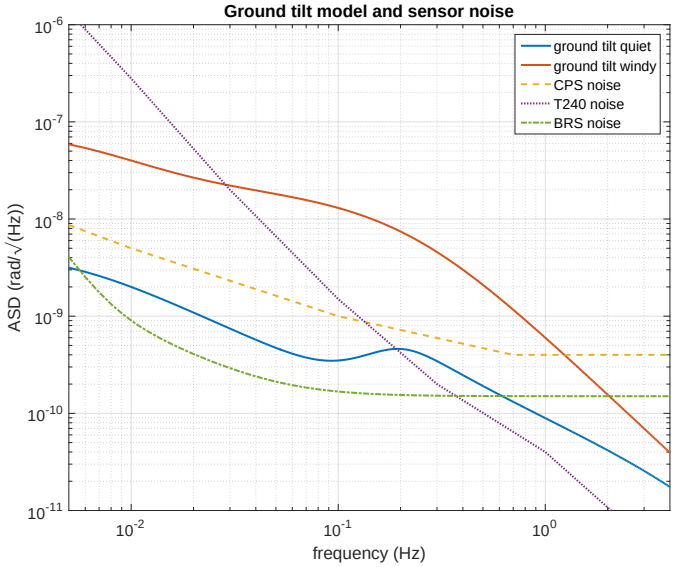

Figure 6. ASD of modeled low and high ground tilt along with tilt sensor noise models for the CPS, T240, and BRS.

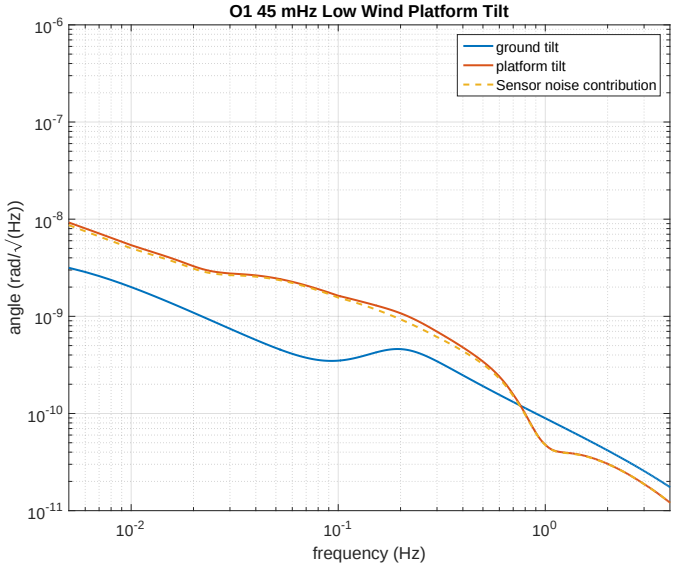

Figure 7. ASD of modeled platform tilt in low wind. Below $\sim$ 500 mHz the control performance is limited by the Stage 1 CPS sensor noise.

filter. However, the sensor noise is only a factor of few below the platform motion. Consequently, the differential motion between platforms located close to each other is close to being limited by the sensor noise.

When wind speeds increase, the ground tilt and consequently the platform tilt increases significantly as shown in Fig. 9. As a result of this increased platform tilt, the platform motion increases by a factor of $\sim$ 20 at 50 mHz as shown in Fig. 10. The increased low-frequency platform translation leads to an increase in the angular motion of the suspended mirrors through length to angle cross-couplings, which are difficult to track down and reduce. The increased angular motion is often responsible for the lockloss since these loops have small bandwidths in order to minimize noise in the gravitational wave band.

In comparison, Fig. 11 shows the platform's translation response under the O2 configuration. Note that the platform tilt response would be identical to that in the O1 configuration since the blends were the same. The platform's isolation above 1 Hz and near the microseism is similar as before, but the isolation is degraded between 0.2 to 0.7 Hz. The gain peaking near 60 mHz is also comparable to before. However, the sensor noise contribution, mainly comprised of the CPS tilt, is suppressed significantly at low frequencies. This configuration has the signficant advantage of the platform motion being dominated by ground motion in this band, which has been found to be mostly common-mode microseismic motion over the 4-km arms as seen in Fig. 1. Thus, the differential platform motion is reduced to a larger extent.

Fig. 12 shows the platform performance under windy conditions, where the benefit from the tilt sensor is most visible. The tilt contribution to the platform motion is suppressed by more than an order of magnitude in the $20 - 100$ mHz range and the overall platform motion is signficiantly reduced. The ground tilt still dominates the

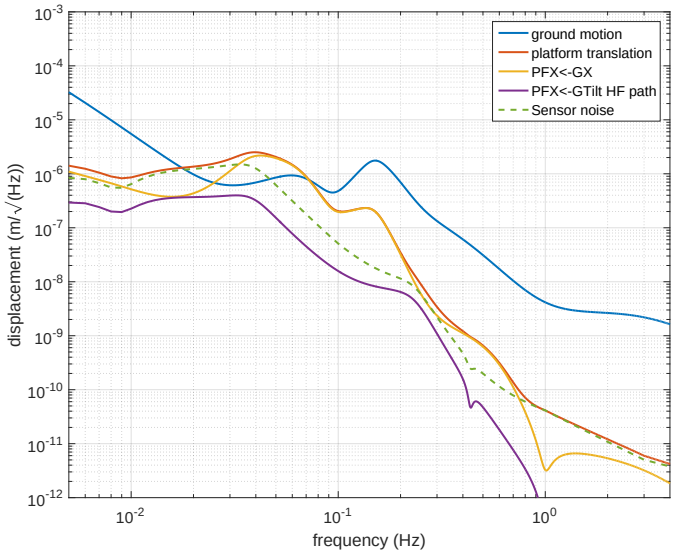

Figure 8. ASD of modeled platform translation during low wind in the O1 configuration. The yellow and purple curves represent, respectively, platform translation cause by ground translations and ground tilts while the red curve represent the residual platform translation.

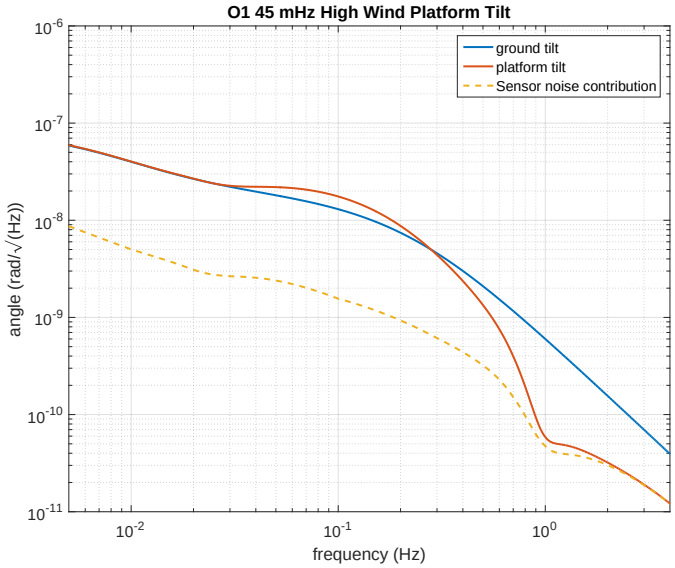

Figure 9. ASD of modeled platform and ground tilt in high wind.

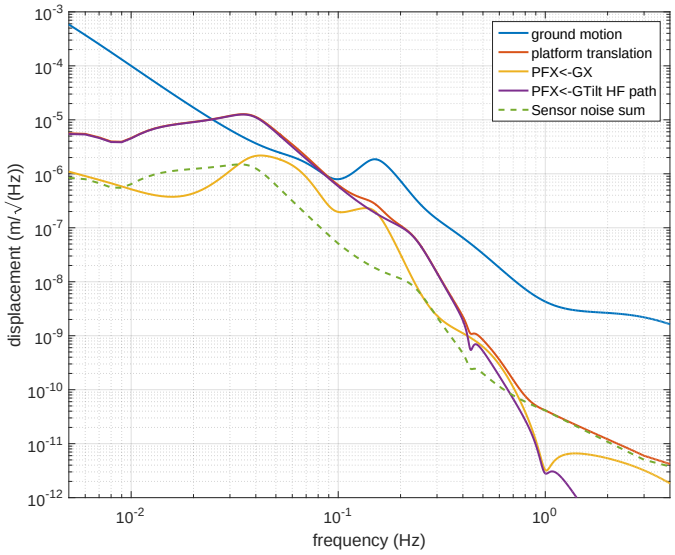

Figure 10. Platform translation in high wind in the O1 configuration.The yellow and purple curves represent respectively platform translation cause by ground translations and ground tilts while the red curve represent the residual platform translation.

platform motion between $0.2 - 0.4$ Hz due to the lack of a reliable rotation sensor on the platform.

3. Comparison with Measured Data

The model in the previous section allows a calculation of the platform motions given the input ground translation and tilts. In reality, we measure ground acceleration with seismometers, which is a combination translation and tilt/rotation, and ground rotation with the rotation sensor. However, it has been found that while translation at these frequencies is coherent over large distances, tilt is coherent only over $\sim$ a few meter distance scales, especially under windy conditions due to the local deformation of the floor slab. Thus, while tilt can be efficiently subtracted from a nearby seismometer, the ground tilt measurement cannot be effectively used for feedforward control of the platform rotation due to the $5 - 7$ meter separation between the platform and the location of the rotation-sensor. Physical obstacles did not allow the sensor to be placed closer to the chamber.

Despite these issues, as the model above suggests, the seismic isolation of the platforms was improved by using the tilt-subtracted ground translation signal. To test the model, we compare the model predictions against measured platform motions during O2. Fig. 13 shows the measured and modelled platform tilt during windy conditions during O2. The first two curves are the measured T240 and CPS tilt sensors on the platform, which show the isolation above the blend frequency of $\sim$ 250 mHz. The next two curves show the predictions of the model based on the measured

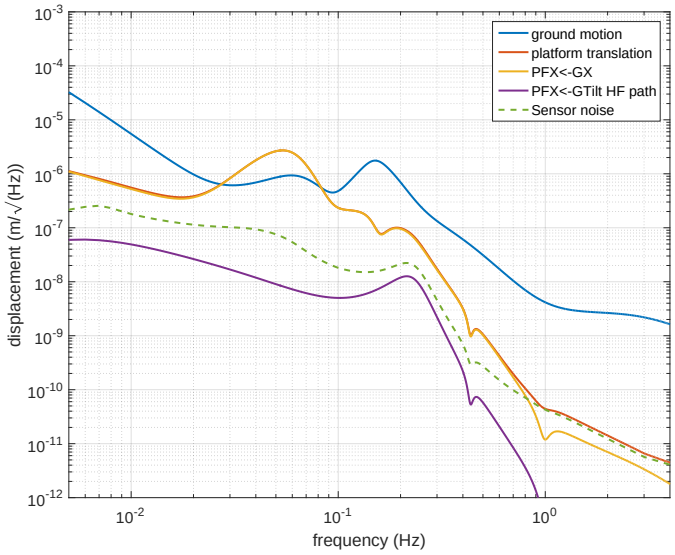

Figure 11. Platform translation in low wind in the O2 configuration.The yellow and purple curves represent respectively platform translation cause by ground translations and ground tilts while the red curve represent the residual platform translation.

ground tilt. The qualitative agreement is quite good, given that we expect there to be differences between the measured ground tilt near the rotation sensor and that near the test mass chamber.

Similarly, Fig. 14 shows the measured and modelled platform translation during windy conditions in O2. As before, the first two curves are the measured T240 and CPS translation sensors on the platform, which show the isolation above the blend frequency of $\sim$ 250 mHz and the extra isolation due to the sensor correction at lower frequencies. The next two curves show the predictions of the model based on the measured ground translation and tilt. Once again, the qualitative agreement is quite good.

Finally, Fig. 15 compares the platform motion as sensed by the CPS sensors during O2 and O1 under very similar (high) wind speeds. The ground motion as measured by seismometers was similar, yet the low-frequency motion during O2 was reduced by nearly an order of magnitude near 50 mHz as compared to O1. This feature is also apparent when comparing the O2 and O1 models and is attributed to the significant decrease in ground tilt coupling to platform translation.

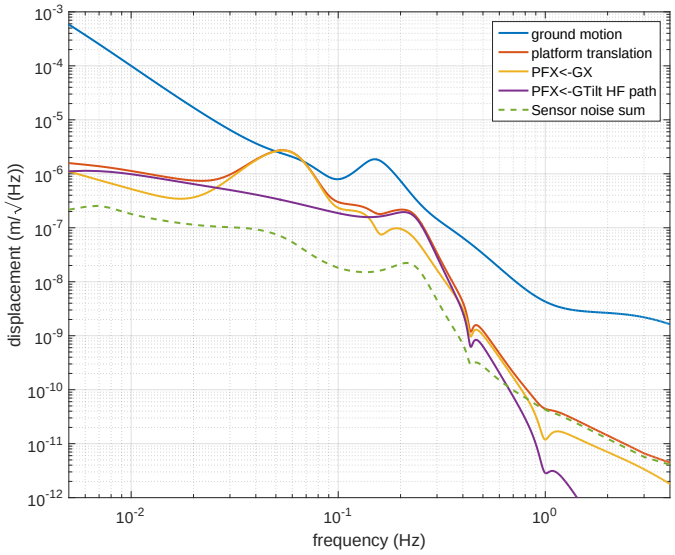

Figure 12. Platform translation in high wind in the O2 configuration. The yellow and purple curves represent respectively platform translation cause by ground translations and ground tilts while the red curve represent the residual platform translation.

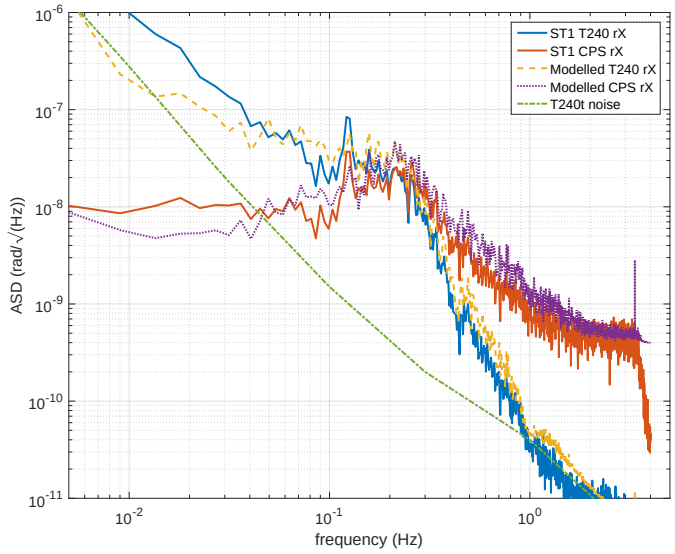

Figure 13. Comparison of measured platform tilt to modelled tilt in high wind in the O2 configuration.

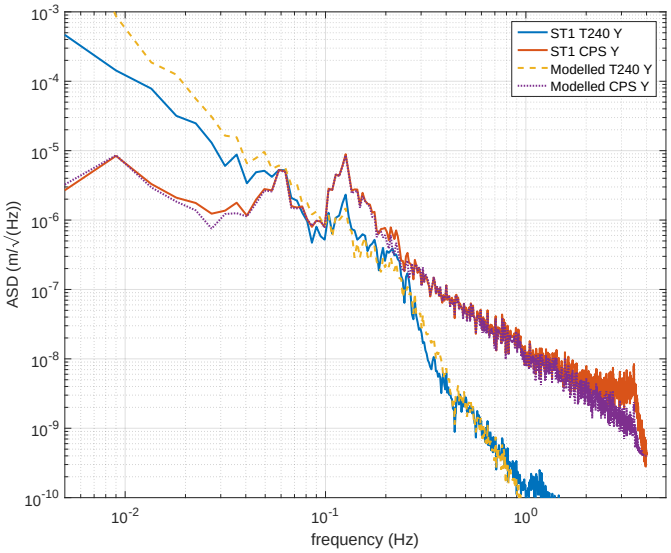

Figure 14. Comparison of measured platform translation to modelled translation in high wind in the O2 configuration.

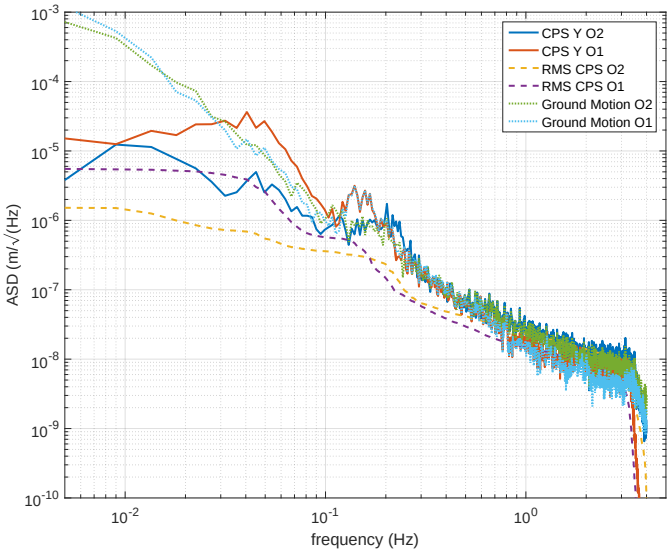

Figure 15. Comparison of measured platform position sensors (CPS) in high wind between the O1 and O2 configuration.

4. Impact on Duty-Cycle and noise

The reduced platform motion under windy conditions has been observed to make lock acquisition easier, as expected. The impact of the O2 configuration on the duty cycle

can be assessed by evaluating the fraction of the time the interferometer was in the locked state as compared to the unlocked state, for a given wind speed. Histograms of the locked fraction are shown in Fig. 16 for the O1 and O2 configurations. The improvement to the duty cycle in O2 is evident above 5-7 mph winds. It is also interesting to note that the locked fraction appears to drop nearly linearly with wind-speed in O1 configuration, whereas in O2 it is nearly independent of wind-speed up to about 15 m/s, after which it falls off steeply due to increased residual tilt contamination.

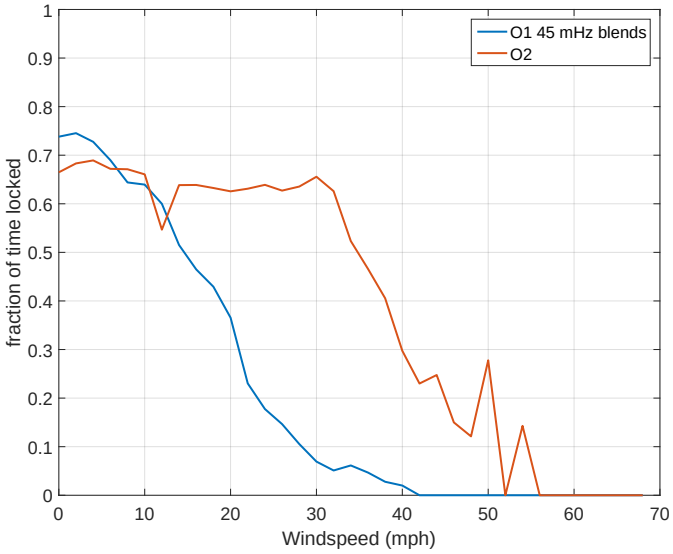

Figure 16. Histogram of fraction of the time the interferometer was locked as a function of wind speed for the O1 and O2 configuration.

5. Summary

The paper discusses the effect of ground tilt on active seismic isolation in LIGO. We have presented a simple analytical model to show the impact of tilt on platform motion in two configurations and shown the benefit of using a ground rotation sensor. The model's predictions agree well with measurements. The use of the ground-rotation-sensors has made the active isolation system less vulnerable to wind-induced tilt and improved the duty cycle of the LIGO Hanford Observatory significantly during wind speeds exceeding 7 m/s. Similar duty cycle improvements are expected to accompany the planned addition of ground rotation sensors at LIGO Livingston Observatory.

6. References

[1] Abbott B P *et al.* (LIGO Scientific Collaboration and Virgo Collaboration) 2016 *Phys. Rev. X* **6**(4) 041015 URL `https://link.aps.org/doi/10.1103/PhysRevX.6.041015`

[2] Abbott B P *et al.* (LIGO Scientific Collaboration and Virgo Collaboration) 2016 *Phys. Rev. Lett.* **116**(13) 131103 URL `https://link.aps.org/doi/10.1103/PhysRevLett.116.131103`
[3] Longuet-Higgins M S 1950 *Philosophical Transactions of the Royal Society of London A: Mathematical, Physical and Engineering Sciences* **243** 1–35 ISSN 0080-4614 (*Preprint* `http://rsta.royalsocietypublishing.org/content/243/857/1.full.pdf`) URL `http://rsta.royalsocietypublishing.org/content/243/857/1`
[4] Matichard F *et al.* 2015 *Classical and Quantum Gravity* **32** 185003 URL `http://stacks.iop.org/0264-9381/32/i=18/a=185003`
[5] Venkateswara K, Hagedorn C A, Turner M D, Arp T and Gundlach J H 2014 *Review of Scientific Instruments* **85** 015005 (*Preprint* `http://dx.doi.org/10.1063/1.4862816`) URL `http://dx.doi.org/10.1063/1.4862816`
[6] Venkateswara K, Hagedorn C A, Gundlach J H, Kissel J, Warner J, Radkins H, Shaffer T, Lantz B, Mittleman R, Matichard F and Schofield R 2017 *Bulletin of the Seismological Society of America* **107** 709–717
[7] Lantz B 2008 *LIGO DCC*

Appendix A.

The two commonly used blend filters are shown in Fig. A1 and A2, labelled as Q250 and R45 blends. The sensor correction filter used in O2 is shown in Fig. A3.

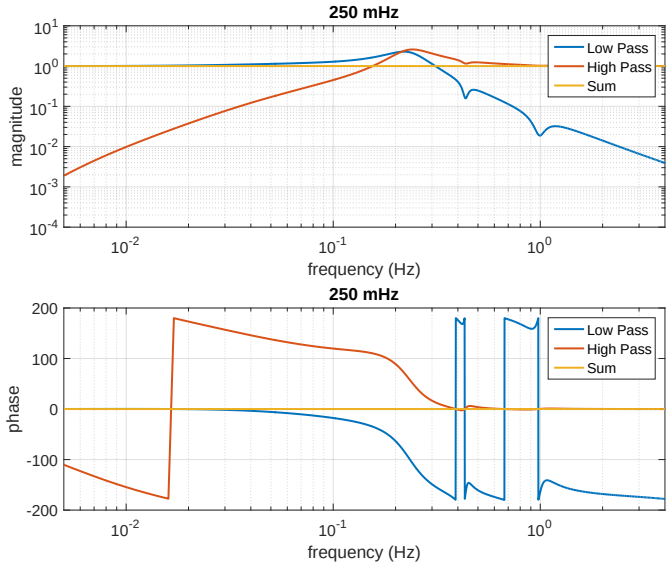

Figure A1. Q250 blend filters.

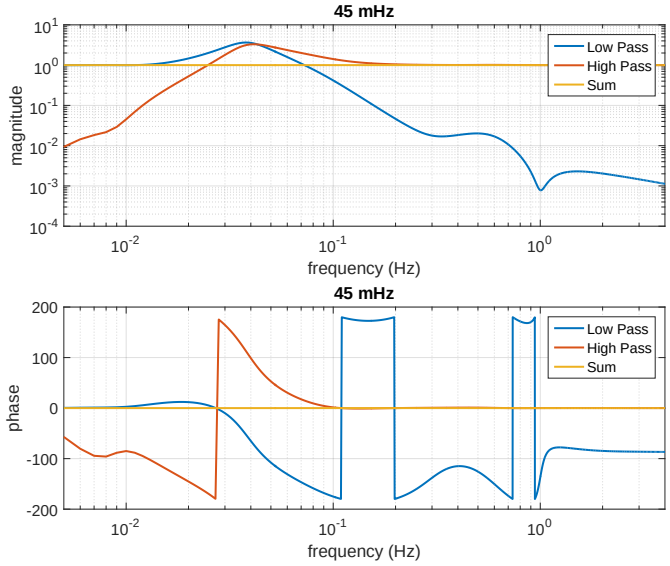

Figure A2. 45 mHz blend filters.

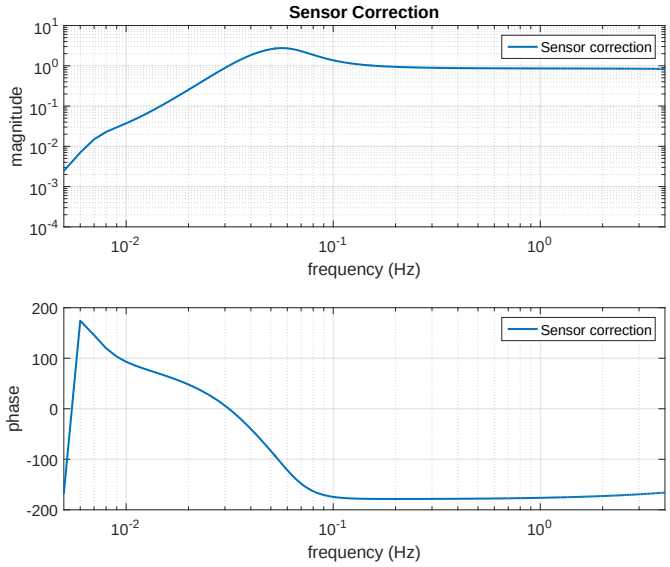

Figure A3. Sensor correction filter.